Optimized sonoreactor for accelerative amyloid-fibril assays through enhancement of primary nucleation and fragmentation

Kichitaro Nakajima [a], Kentaro Noi [b], Keiichi Yamaguchi [a], Masatomo So [c], Kensuke Ikenaka [d], Hideki Mochizuki [d], Hirotsugu Ogi [e,*], Yuji Goto [a,*]

[a] Global Center for Medical Engineering and Informatics, Osaka University, Suita, Osaka 565-0871, Japan
[b] Institute for NanoScience Design, Osaka University, Toyonaka, Osaka 560-8531, Japan
[c] Institute for Protein Research, Osaka University, Suita, Osaka 565-0871, Japan
[d] Department of Neurology, Graduated School of Medicine, Osaka University, Suita, Osaka 565-0871, Japan
[e] Graduate School of Engineering, Osaka University, Suita, Osaka 565-0871, Japan

A R T I C L E   I N F O

A B S T R A C T

Ultrasonication to supersaturated protein solutions forcibly forms amyloid fibrils, thereby allowing the early-stage diagnosis for amyloidoses. Previously, we constructed a high-throughput sonoreactor to investigate features of the amyloid-fibril nucleation. Although the instrument substantiated the ultrasonication efficacy, several challenges remain; the key is the precise control of the acoustic field in the reactor, which directly affects the fibril-formation reaction. In the present study, we develop the optimized sonoreactor for the amyloid-fibril assay, which improves the reproducibility and controllability of the fibril formation. Using β_2-microglobulin, we experimentally demonstrate that achieving identical acoustic conditions by controlling oscillation amplitude and frequency of each transducer results in identical fibril-formation behavior across 36 solutions. Moreover, we succeed in detecting the 100-fM seeds using the developed sonoreactor at an accelerated rate. Finally, we reveal that the acceleration of the fibril-formation reaction with the seeds is achieved by enhancing the primary nucleation and the fibril fragmentation through the analysis of the fibril-formation kinetics. These results demonstrate the efficacy of the developed sonoreactor for the diagnosis of amyloidoses owing to the accelerative seed detection and the possibility for further early-stage diagnosis even without seeds through the accelerated primary nucleation.

1. Introduction

Amyloid fibrils are proteinaceous aggregates with ordered β-sheet structures, exhibiting the diameter and length of approximately 10 nm and a few micrometers, respectively[1]. The fibril formation fundamentally relates to the onset and development of amyloidoses, which are intractable diseases such as Alzheimer's disease and Parkinson's disease [2]. Causative specific proteins are identified in individual amyloidoses. However, a common mechanism governs their onset[3], i.e., soluble protein monomers, which play various biological functions in a healthy body, form insoluble amyloid fibrils and deposit in the physiological tissues, thereby causing malfunction[4,5]. Because tissue malfunction constitutes irreversible damage in most cases, diagnosing fibril-formation risk prior to the onset of clinical symptoms is vital[6].

Fibril formation occurs through the primary nucleation and subsequent fibril growth[7] in the solution, in which protein concentration is above the solubility. It is analogous to the crystallization in a supersaturated solution[8,9]. The supersaturation state is divided into two states in detail, namely labile and metastable states. In the labile state, the solute spontaneously precipitates and grows after a certain lag time. In the metastable state, by contrast, the spontaneous nucleation fails to occur, because the free-energy barrier for nucleation retains the supersaturation. Supersaturation in the metastable state can be broken by external stimuli, such as mechanical agitation or the addition of the crystalline template. This phenomenon is typically seen in the seeding reaction in fibril formation[10]: When the preformed fibrils, so-called seeds, are added to the metastable-state solution as a template, the fibril formation immediately begins[11,12], and it is completed when the soluble protein concentration reaches the solubility[13]. In light of the fact that the seeds trigger the onset of amyloidosis, some research

* Corresponding author.
E-mail addresses: ogi@prec.eng.osaka-u.ac.jp (H. Ogi), gtyj8126@protein.osaka-u.ac.jp (Y. Goto).

groups have reported that investigating the seeding reaction behavior with seeds from biological fluids enables one to distinguish the type of disease[14–16]. In addition to seed detection, further early-stage diagnosis prior to nucleation is desired for completely suppressing nucleation, which is the principal trigger of the amyloidoses. There are multiple reports in the literature regarding factors to promote and inhibit nucleation in vitro[17,18]. However, it is never straightforward to investigate the nucleation risk in vivo because the factors are obscured by supersaturation prior to the nucleation.

We previously revealed that ultrasonication to protein solutions in the metastable state forces the nucleation of amyloid fibrils by forcibly relieving the supersaturation[19]. In the ultrasonication-forced fibril formation, fibrils are formed after a lag time, which depends on the supersaturation condition, from minutes and days[19–21]. Because the lag time reflects the potency of the nucleation, ultrasonication allows us to investigate the nucleation potency of protein solutions by forcibly relieving the supersaturation. In order to leverage the remarkable capabilities of ultrasonication, we previously developed a high-throughput analysis system that utilized ultrasonication-forced fibril formation, referred to as a Handai amyloid burst inducer (HANABI)[21]. In the HANABI, a 96-well microplate containing sample solutions is placed in a water bath and irradiated with an ultrasound generated by Langevin-type transducers. The instrument involves a microplate-reading system for monitoring the fibril formation through the measurement of fluorescence. We used this instrument to investigate the effects of ultrasonication on various proteins, including hen egg-white lysozyme, β_2-microglobulin (β2m), and amyloid-β peptide[21]. The previous work substantiated that ultrasonication is a powerful tool for investigating the propensity for nucleation. However, the HANABI faced several difficulties in achieving high reproducibility of the assay. In general, acoustic field in a sample solution could not be the same because of changes in temperature, the volume of the water, and the distribution of the dissolved gases in the water bath, where the ultrasound propagated to reach the sample solution[22]. In particular, for the amyloid-fibril assay, a long-time ultrasonication over tens of hours leads to significant changes in the water bath condition, deteriorating the reproducibility of the acoustic field that directly affects the fibril-formation reaction. Furthermore, in the previous HANABI system, the fluorescence signal was acquired from the upper surface of the microplate, which was significantly affected by water droplets on the microplate because of the high-power ultrasonication.

In this study, we develop an optimized sonoreactor for the amyloid-fibril assay, named the HANABI-2000, as displayed in Fig. 1. First, we eliminated the water bath in order to conduct a reproducible analysis. A single rod-shaped ultrasonic transducer is placed on each sample solution in an assay plate. The resonant frequency of the transducer is 30 kHz, which is optimized for accelerating fibril formation[23,24]. Second, we placed a microphone below the assay plate to measure the acoustic intensity of each sample solution. The acoustic-intensity measurement allows us to control the acoustic field in each well by individually controlling the voltage and frequency of the driving signal applied to each transducer. Third, we placed a photodetector beneath the microplate to measure the fluorescent signal, which improves the signal-to-noise ratio of the fluorescence measurement because of the absence of the water bath. Using this instrument, we perform fibril formation and seed detection experiments for β2m, which has been widely investigated due to the clinical importance in dialysis-related amyloidosis[25,26]. In the experiment, a fibril formation of β2m supersaturated solution is induced by optimized ultrasonication to break the supersaturation. The compensation of the acoustic field in each sample solution results in identical fibril-formation behavior in the 36 independent solutions. Moreover, the seed detection experiment is performed to demonstrate the applicability of the HANABI-2000 to the clinical diagnosis: We succeed in detecting the ultra-trace seeds with a concentration of 100 fM, which is much lower than the solubility (26 nM)[13], at an accelerated rate. The result confirms the efficacy of the HANABI-2000 in a clinical situation. The analysis, based on chemical kinetics, reveals that the fibril-formation acceleration is attributed to enhanced primary nucleation and the fibril fragmentation. These results demonstrate the viability of the HANABI-2000 for the accelerative seed detection assay and the investigation of risk factors to nucleation that are necessary for the further early-stage diagnosis of amyloidoses prior to the nucleation.

2. Materials and methods

2.1. Construction of HANABI-2000

We constructed a sonoreactor for the amyloid-fibril assay, which we named HANABI-2000[27], as illustrated in Fig. 1. The entire systems were integrated within a space of $500 \times 550 \times 550$ mm^3, as shown in Fig. 1(a). The device comprises three systems, namely a transducer
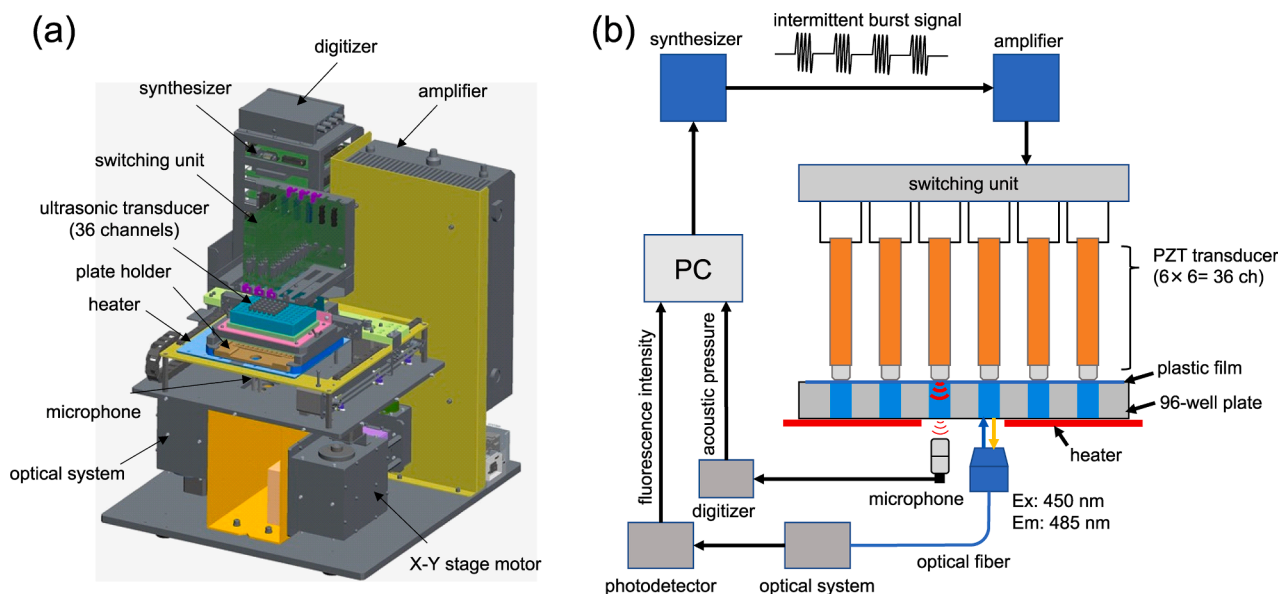

Fig. 1. (a) 3D schematic illustration of the optimized sonoreactor for the amyloid-fibril assays, the HANABI-2000 (HANdai Amyloid Burst Inducer 2000). The dimensions of the device are $500 \times 550 \times 550$ mm^3. (b) Block chart of the control units of the HANABI-2000.

driving system, an acoustic-intensity measurement system, and a fluorescence measurement system. A block chart is shown in Fig. 1(b). 36 piezoelectric lead zirconate titanate (PZT) transducers are placed on a commercially-available 96-well plate, including sample solutions. Note that the number of transducers can, in principle, be increased to 96. A plastic film with a thickness of 0.1 mm (WATSON, 547-KTS-HC) is used to seal the solutions, and the transducers are contacted with the plastic film without any acoustic coupling materials, through which the ultrasound is generated within the solution. All transducers are connected to the signal switching unit and then sequentially driven by a burst signal. The frequency and amplitude of the burst signal are individually controlled. The generated burst signal is amplified by the amplifier (NF instruments, BA4825) and sent to each transducer through the switching unit. The burst length is 300 ms, and the time required for switching is 500 ms. Therefore, the 300-ms ultrasonication in a single well is sequentially performed every 29 s. The resonant frequency of each transducer is separately determined by sweeping the driving frequency and measuring the acoustic intensity by the microphone (PCB Piezotronics, 378C01) placed below the assay plate.

We adopt a thioflavin-T (ThT) fluorescence assay for evaluating the time course of fibril formation. Because ThT molecule specifically binds to the β-sheet structure of the fibrils and emits high-intensity fluorescence[28], an increase in the ThT fluorescence intensity corresponds to the increase in formed fibrils. Then, we incorporated a fluorometer with excitation and detection wavelengths of 450 and 485 nm in the HANABI-2000. The excitation light is emitted from a xenon lamp (HAMAMATSU PHOTONICS K. K., L2436) and irradiates the sample solution from below via an optical fiber.

2.2. Preparation of the sample solution

The wild-type β2m monomer was expressed in *Escherichia Coli* (BL21) and purified, as previously described[29]. The purified β2m was lyophilized and stored at $-20\,°$ C until just before the experiment. The lyophilized β2m monomers were then dissolved into ultrapure water, after which the solution was filtrated by a membrane filter with a pore diameter of 220 nm (Millipore, SLGVR04NL) to decontaminate preformed aggregates, if any. The concentration of the β2m monomer was determined through the absorbance measurement using its absorbance coefficient at 280 nm of 1.93×10^4 $M^{-1}cm^{-1}$. In the fibril-formation experiment, the sample solution includes a 25.4 μM (0.3 mg/mL) β2m monomer, 20 mM HCl, 150 mM NaCl, and 5μM ThT. In the seeding experiment, we first prepared seed solutions by breaking down the preformed fibrils using the ultrasonic homogenizer (Misonix, XL-2000) for 1 s 5 times and diluting to intended concentrations with a 10 mM HCl. We then mixed them with the monomer solution to prepare the sample solutions with different seed concentrations. The final sample solutions include a 2.54 μM (0.03 mg/mL) β2m monomer with the above-described concentrations of HCl, NaCl, and ThT, and different concentrations of β2m seeds between 100 fM to 100 nM. (Note that this concentration corresponds to concentration of monomers constructing the seeds.) The total time needed to prepare the sample solution was about 30 min. It should be noted that the solubility of β2m is 26 nM (0.3 μg/mL)[13], and the prepared solutions are in supersaturation. In contrast, the monomer concentration in some seed solutions was below the solubility, and the seeds there would be dissolved eventually[30]. However, because the depolymerization of seeds proceeds slowly[31], the seed dissolution could be negligible by the immediate addition of the seeds to the supersaturated monomer solution following dilution. The seed activity, with a concentration of less than the solubility, is outlined in the Results and Discussion section.

2.3. Assay in HANABI-2000

The prepared sample solution was dispensed into a 96-well plate

(Eppendorf, Microplate 96/F) with a volume in each well of 395 μL, after which the plastic film was carefully attached to the plate to avoid bringing air bubbles into the well. The prepared plate is set on the plate holder of the HANABI-2000, and the ultrasonic transducers are pushed against the plastic film. The resonant frequency of each transducer was determined by means of the acoustic intensity measurement using the microphone. The sample solution temperature was set to 37 °C throughout this study using a heater embedded in the plate holder. During the assay, the HANABI-2000 automatically irradiates the sample solutions with the optimized ultrasound and records their fluorescent intensities every 10 min.

2.4. AFM measurement

After the assay, the sample solution was diluted for 10 folds with ultrapure water, and its droplet was placed on a mica plate. After the surface was dried, AFM images were acquired using a HITACHI AFM5000II system in the tapping mode.

2.5. Theoretical analysis of fibril formation kinetics

The theoretical model based on the chemical kinetics[32] is used for the detailed analysis of the experimental ThT time course, which allows us to independently calculate the rate constant of the three reaction pathways, the primary nucleation, the fibril growth, and the fragmentation of mature fibrils. Detail about each of the reaction pathways is provided in the Results and Discussion section. In the model, the fibril mass concentration at a time $t, M(t)$, is described as

$$M(t) = m_{tot}\left\{ 1 - \exp\left(-C_+e^{\kappa t} + C_-e^{-\kappa t} + \frac{k_n}{m_{tot}^{n_c}k_-} \right) \right\}, \quad (1)$$

where $\kappa = \sqrt{2m_{tot}k_+k_-}$ and $C_{\pm} = \frac{k_+P_0}{\kappa} \pm \frac{M_0}{2m_{tot}} \pm \frac{k_n m_{tot}^{(n_c-1)}}{2k_-}$. Here, $m_{tot} = 2.54$ μM, $n_c = 2, P_0$, and M_0 denote the initial monomer concentration, the size of the critical nuclei, the initial seed number concentration, and the initial seed mass concentration. In turn, k_n, k_+, and k_- are the rate constants for the reaction pathways of the primary nucleation, fibril growth, and fragmentation, respectively. The three rate constants are determined inversely via the global fitting between the theoretical and experimental fibril-formation time course under various seed concentrations, where P_0 was assumed to be $P_0 = M_0/1000$ and the initial values of k_n, k_+, and k_- in the fitting were used as common values for all of the datasets as follows: $k_n = 1.0 \times 10^{-15}$ $M^{-1}\cdot s^{-1}, k_+ = 1.0 \times 10^4$ $M^{-1}\cdot s^{-1}$, and $k_- = 1.0 \times 10^{-9}$ s^{-1}.

3. Results and discussion

3.1. Ultrasonication characteristics of HANABI-2000

A rod-shaped PZT transducer, as shown in Fig. 2(a), was incorporated in the HANABI-2000. The transducer equips a quartz part at the tip to smoothly make contact with the plate's surface. The size of the PZT transducer is $4.24 \times 4.24 \times 54$ mm^3, which was determined so as to show the optimum resonant frequency of 30 kHz using the finite element method (FEM) simulation. (We previously revealed that the 30 kHz ultrasonication significantly accelerates the fibril formation[23].) As shown in Fig. 2(b), the transducer resonates in the longitudinal direction (the *x*-axis in Fig. 2(b)) by the transverse piezoelectric effect. The PZT material (P213-C, Fuji Ceramics Corp.) possesses a piezoelectric constant d_{31} of -1.39×10^{-10} m· V^{-1}. Fig. 2(c) displays the resonant spectra of the transducer, whose resonant frequency is ~ 30 kHz as designed, in the situation under contact with the plate including the sample solutions. The peak intensity increases as an increase in the applied voltage.

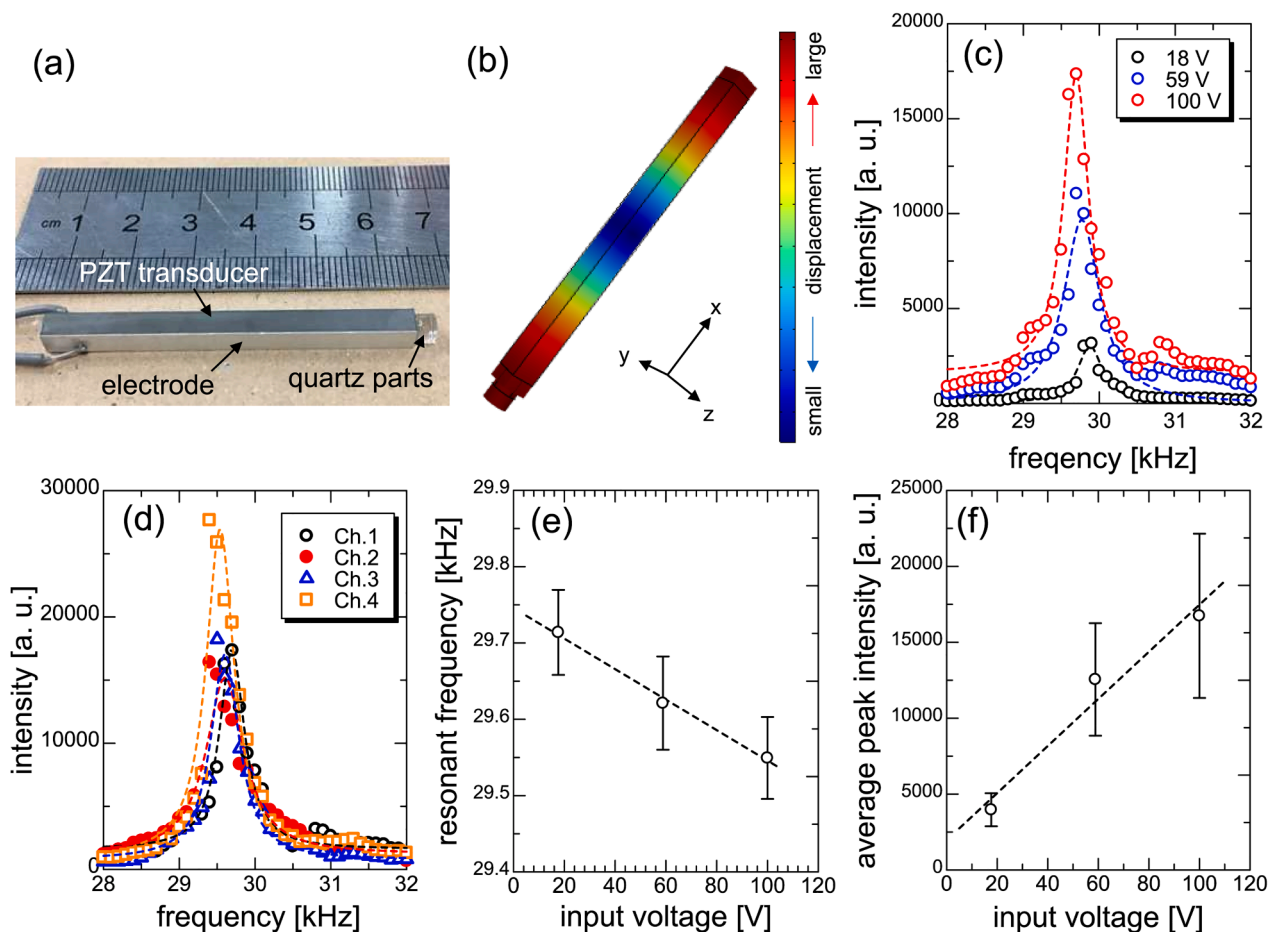In this study, we used 36 transducers and independently controlled

Fig. 2. (a) Visual depiction of the PZT transducer used in the HANABI-2000. (b) FEM simulation result for the resonant-frequency estimation of the PZT transducer with the dimensions of $4.24 \times 4.24 \times 54$ mm^3. The solid black line depicts an outline of the transducer prior to the deformation, which indicates the resonance in the longitudinal direction (*x*-axis). (c) The resonant spectra of the PZT transducer with different applied voltages, with the dashed lines representing the fitting curves of the Lorentz function. (d) The resonant spectra of four different transducers with the applied voltage of 100 V, which indicates the difference in the resonant characteristics. The average and deviation of (e) the resonant frequency and (f) the peak acoustic intensity across all 36 transducers. The error bars denote the standard deviation.

the acoustic conditions in the individual wells. Because the ultrasonication-forced fibril formation highly depends on the acoustic conditions[21,23,33], the acoustic-field deviation within each well is crucial to achieving a uniform assay. Indeed, the transducers exhibited different resonant spectra, even under the same applied voltage, as shown in Fig. 2(d), which is attributed to a difference in the contact condition between the transducer tip and plate surface. We then performed an acoustic intensity measurement for all 36 transducers in order to evaluate the deviation of the resonant frequency and peak intensity under different applied voltages (18, 59, and 100 V), as shown in Fig. 2 (e) and 2(f), respectively: The resonant frequency exhibited a standard deviation of less than 0.1 kHz, independent of the applied voltage. As indicated by the result, the resonant frequency shifted slightly to a lower frequency as an increase in the applied voltage, which was inferred to be attributable to an increase in an energy loss within the material. The peak intensity should be a primary factor in the fibril formation reaction, because the acoustic frequency was almost the same within all of the wells. The fibril formation shows a gentle frequency dependency in the range from 20–250 kHz[23], which implies that the fibril formation is insensitive to frequency changes of the order of 0.1 kHz. Then, we focused on tuning the difference in the peak intensity shown in Fig. 2(f) by controlling the applied voltage. The applied voltage was independently compensated for being the same peak intensity in each well. The effectiveness of the compensation is discussed in the next section.

3.2. Fibril formation in the β2m monomer solution

We performed the fibril-formation experiments in the β2m monomer solution by means of the HANABI-2000. Because the β2m monomer forms the amyloid fibril under acidic conditions with ultrasonication [19,34], a β2m supersaturated monomer solution under the acidic condition was prepared for this assay. Spontaneous fibril formation failed to occur without ultrasonication within 30 h, as shown by the black curves in Fig. 3(a). In the ultrasonicated samples (the red curves in Fig. 3(a)), the time-course curves of the ThT fluorescence intensity showed a precipitous increase following the lag time, being a typical sigmoidal curve of the fibril formation[28]. Furthermore, the AFM image of the ultrasonicated sample showed typical fibril morphology in the formed aggregates, as shown in the inset of Fig. 3(a). These results demonstrate that the HANABI-2000 succeeded in inducing the β2m fibril formation.

Next, we evaluate a deviation in the fibril-formation reaction under ultrasonication. Fig. 3(b) presents 36 ThT curves of the ultrasonicated samples taken without the aforementioned compensation procedure. Here, the ThT fluorescence intensity was normalized by the maximum value of each sample to compare their fibril-formation behavior. Without compensation, all transducers were driven by the applied voltage of 150 V and frequency of 29.5 kHz. As a result, the ThT curves shows a variety of time-course behaviors; the samples with the relatively long lag time ($t_{half} > 5$ h) exhibited a sigmoidal curve, where t_{half}
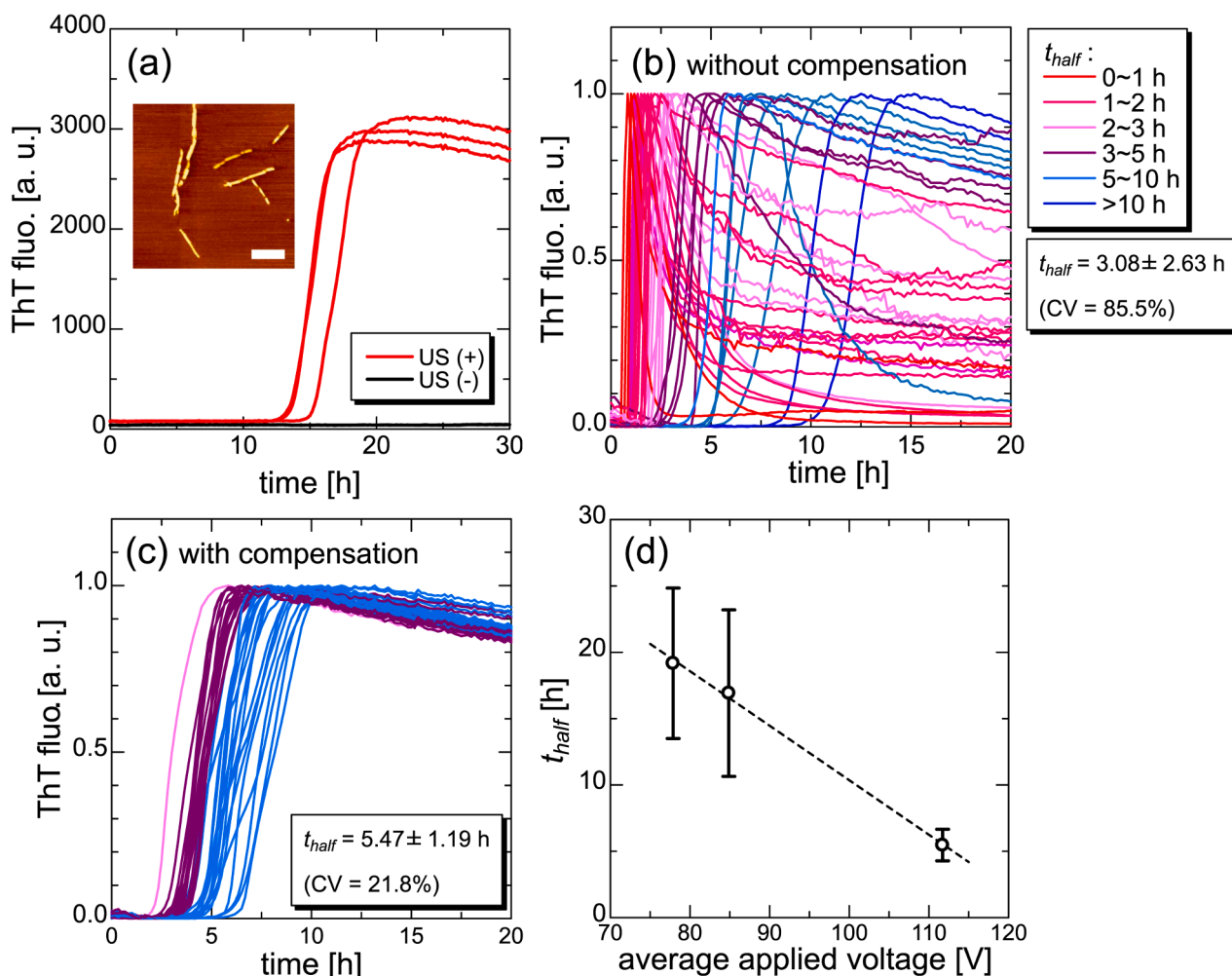
Fig. 3. (a) Time-course curves of the ThT fluorescence intensity of the acidic β2m monomer solution with (US (+), red curves) and without ultrasonication (US (-), black curves). The inset shows an AFM image of the aggregates formed by ultrasonication. The scale bar denotes 500 nm. The ThT time-course curves ($n = 36$), which are irradiated with the ultrasound (b) without and (c) with the compensation procedure. The compensation clearly improves the variation in the ThT time-course behavior. (d) Relationship between the applied voltage and t_{half} in three independent experiments, showing their inverted correlation.

denotes the time that the ThT intensity reached at half of the maximum value. In contrast, the samples with the short lag time ($t_{half} < 2$ h) display the spike-like ThT behavior, which is composed of the first sharp increase and subsequent decrease in the fluorescence intensity. Our previous studies indicate that the spike-like curve is caused by the denaturation of the formed fibrils into ThT-negative aggregates under excessively strong ultrasonication[35,36], which was often seen in assays that make use of previous version of HANABI[21]. Although t_{half} usually reflects the propensity for fibril formation of the sample solution, the fibril formation under overstrong ultrasonication is only governed by the acoustic condition. This is unfavorable for clinical applications, which investigate the aggregation potency of the biological samples. Furthermore, of the 36 wells, t_{half} showed a large variation with a coefficient of variation (CV) of 85.5 % across all of the samples.

In order to achieve a uniform assay while avoiding the undesirable effect of excessive ultrasonication, the compensation procedure was adopted, which independently set the applied voltages to between 59 and 150 V based on the acoustic-intensity-measurement results. As shown in Fig. 3(c), all 36 time-course curves show the identical sigmoidal behavior. Furthermore, the variation of t_{half} is improved to be 5.47 ± 1.19 h with a CV of 21.8%. The CV value is reasonable in the uniform fibril-formation assay, because fibril formation intrinsically comprises a large deviation in the lag time[21]. In the previous HANABI, a CV of $\sim 20\%$ was achieved by moving the assay plate across the plane

of a wide water bath surface during the 1-min ultrasonication[21]. However, the ThT time course showed spike-like shape. In the HANABI-2000, the equivalent uniformity is achieved through the compensation of the applied voltage featuring a preferred sigmoidal behavior. The higher the applied voltage, the shorter the t_{half}, as shown in Fig. 3(d), in which the tendency is consistent with the findings of previous studies [23,33]. This fact indicates that the HANABI-2000 can independently control the fibril-formation reaction at each well by means of the compensation procedure.

3.3. Accelerative β2m seed detection

Some research groups have previously reported that seed detection in biological samples, such as cerebrospinal fluid and brain lysate, contributes to the diagnosis of amyloidoses[15,16]. Therefore, we performed a seed detection experiment in order to confirm the viability of the HANABI-2000 for diagnostic purposes. The seed concentration in the biological samples is ultra-trace; concerning the β2m, its blood concentration is of the order of 1 μM (10 μg/mL) in dialysis patients, who face the risk of dialysis-related amyloidosis[37]. It is inferred that a small portion of monomers form the seeds, implying that the seed concentration should be much lower than the monomer one. Based on this fact, we used the β2m seeds with the concentration in the range from 100 fM to 100 nM in 10-fold increments.

In the sample with the 10-nM seed, the fibril formation began immediately even without ultrasonication, as shown by the black curves in Fig. 4(a); this tendency is generally seen in the seed-dependent fibril-formation reaction[38]. Ultrasonication further accelerates the evolution of fibril formation, even in the seed-dependent reaction. It should be noted that the seed concentration of 10 nM is lower than the solubility (26 nM). Although the 10 nM seeds would be dissolved into the solution after a long incubation, the immediate addition procedure (see the Materials and Methods section) keeps the seed activity even in concentration below solubility.

The fibril formation occurred after a lag time of ~ 25 h in the lower seed concentration of 100 pM without ultrasonication, as shown in Fig. 4 (b). The lag time is shortened by ultrasonication from 25 h to 8 h by means of the acceleration effect. With a relatively high seed concentration above 10 nM, the fibril formation began without a lag time because the seed effect rapidly propagated throughout the entire solution. Even when the seed amount is insufficient to fully remove the lag time, the seeding reaction locally proceeds through the solution, which resulted in a shorter lag time than that of a pure monomer solution. Although the fibril formation was not observed within 40 h without ultrasonication in the samples with 100 fM seeds (Fig. 4)) and without the seeds (Fig. 4(d)), in these conditions ultrasonication induced fibril formation. Because t_{half} reflects solution's propensity for fibril formation, the average t_{half} of the solution with 100-fM seeds is shorter than that without the seeds.

The correlation between the seed concentration and t_{half} is summarized in Fig. 4(e). t_{half} correlates to the seed concentration in a logarithmic manner in the range from 100 fM to 100 nM, which is consistent with previous reports[39]. This fact demonstrates that the HANABI-2000 allows us to quantify the seed concentration with the dynamic range of seven orders of magnitude. In terms of the seed detection limit (SDL), the t_{half} of the sample with 100 fM seeds is clearly separated from that of the sample without seeds, which indicates an SDL of less than 100 fM. Moreover, the slope of the fitted logarithmic curve reveals the accelerative rate in the seed detection in the HANABI-2000 by a factor of 3 compared to that without ultrasonication. These results demonstrate

the applicability of the HANABI-2000 to clinical diagnosis through the accelerative seed quantification with an SDL of 100 fM or less.

3.4. Acceleration mechanism of fibril formation in the HANABI-2000

During fibril formation under ultrasonication, three reaction pathways may contribute to fibril-formation kinetics: (i) Primary nucleation, where the monomers associate with one another to assemble the critical nuclei beyond the nucleation free-energy barrier; (ii) Fibril growth, whereby the monomers attach to the formed fibrils to grow the fibril molecules. The addition of the monomer only occurs at the fibril termini [10], which implies that the fibrils grow in the form of a one-dimensional crystal; (iii) Fragmentation, where a single mature fibril can fragmentate into multiple shorter fibrils, because it is breakable filament[32,40,41]. The fragmentation pathway secondarily increases the active seeds.

We here adopt the theoretical model based on the chemical kinetics using the three aforementioned pathways[32] to discuss the acceleration mechanism in the HANABI-2000. It should be noted that all soluble monomers ultimately transform their state into insoluble fibrils in the theoretical model. However, fibril formation is essentially a supersaturation-limited phase transition[34,42,43], which indicates that the soluble monomer concentration must be its solubility after the entire solution reaches equilibrium through the fibril-formation process. Previously, we experimentally demonstrated that the β2m solubility under acidic conditions is 26 nM[13]. Because the solubility is $\sim 1\%$ for the initial monomer concentration in our experiments, we approximately applied the theoretical model to the analysis on basis of the assumption that the contradiction does not fundamentally affect fibril-formation behavior.

Fig. 5(a) and 5(b) represent the global fitting results between the theoretical and experimental fibril-formation kinetics with and without ultrasonication under different seed concentrations. The comparison between the rate constants with and without ultrasonication reveals that k_n and k_- are significantly enhanced by ultrasonication by a factor of 1200 and 15.8, respectively. In contrast, k_+ remains of the same order
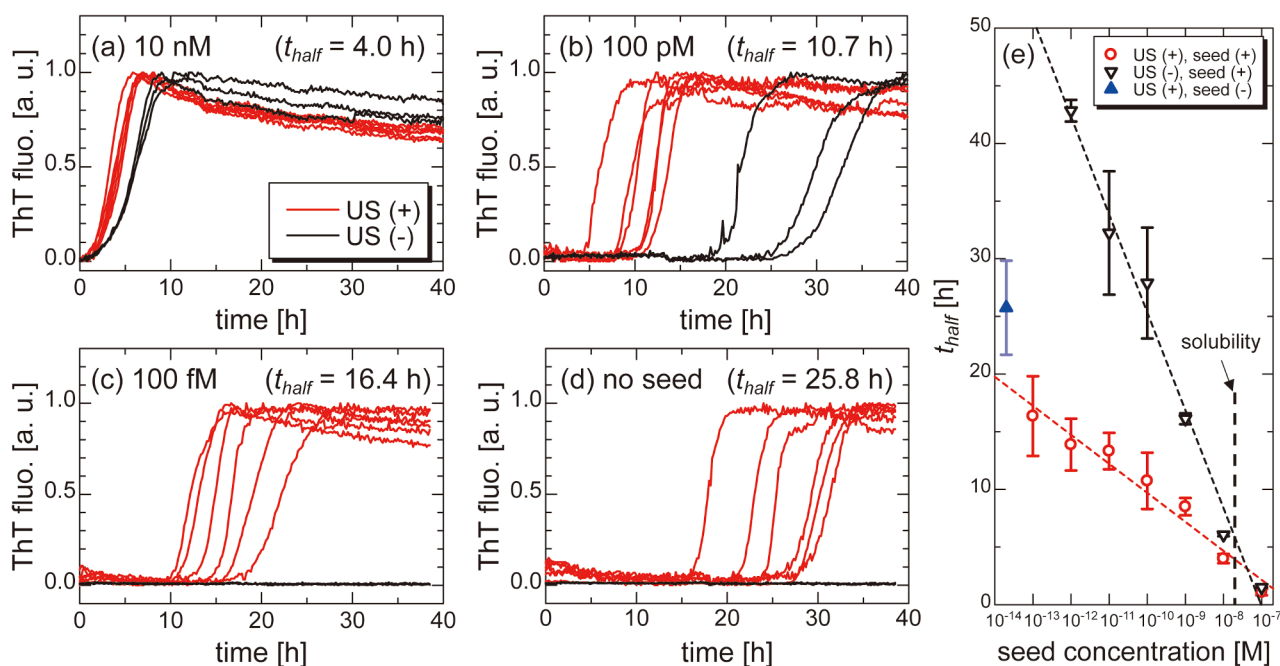

Fig. 4. ThT time-course curves of the samples with (a) 10 nM, (b) 100 pM, and (c) 100 fM seeds, and (d) without the seeds. The red and black lines denote the samples with (US (+), $n = 6$) and without (US (-), $n = 3$) ultrasonication, respectively. The t_{half} in each panel is the averaged value among the six samples with ultrasonication. (e) The relationship between the seed concentration and t_{half}. The dashed lines are the fitted curves as depicted by a logarithmic function. The solubility of β2m is 26 nM under the acidic condition[13], which is depicted by the black broken line.
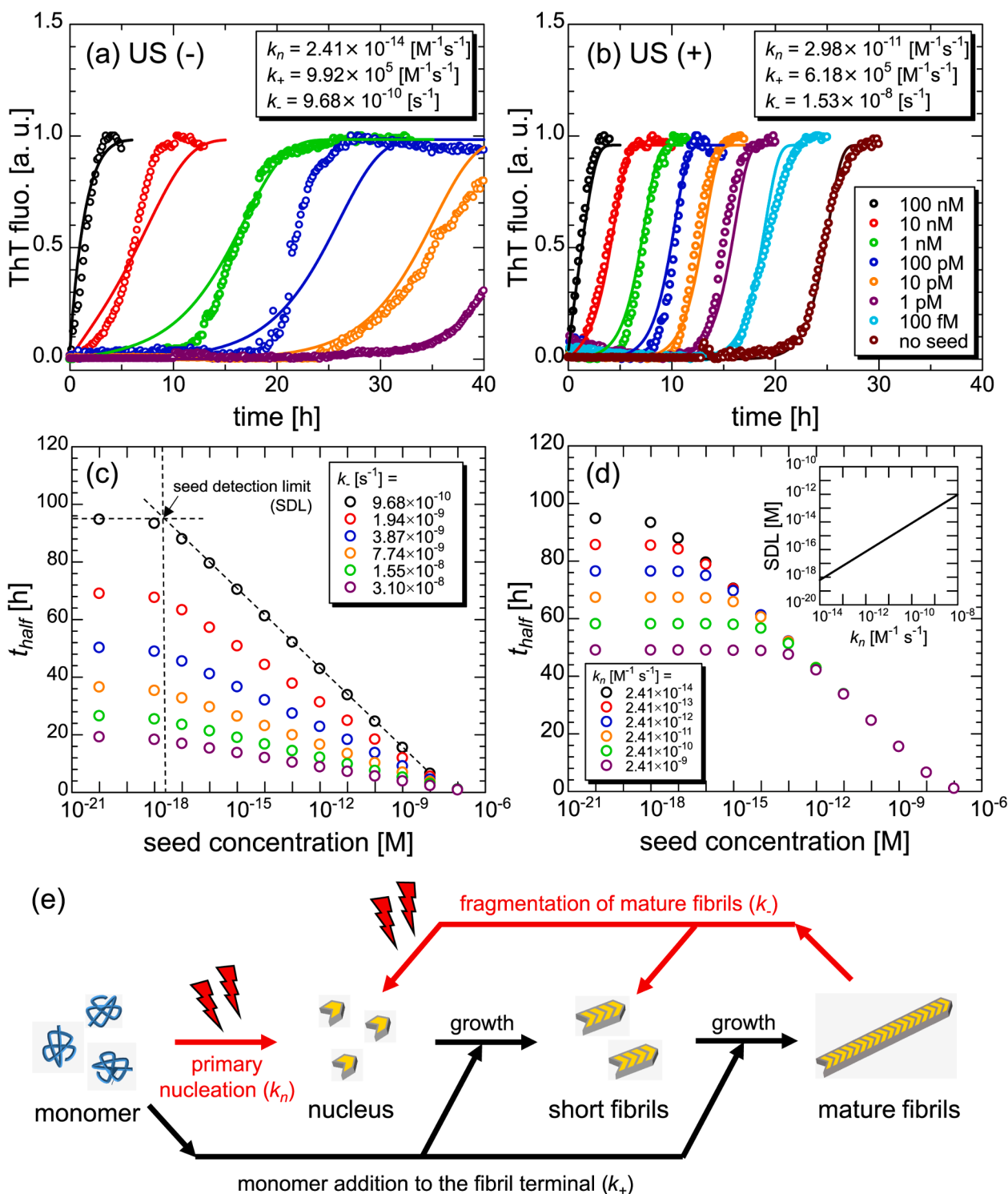
Fig. 5. Analysis of the fibril-formation kinetics with different seed concentrations by the theoretical model (a) without (US(-)) and (b) with ultrasonication (US(+)). The color of each curve in (a) corresponds to the legend in (b). $k_n, k_+,$ and k_- denote, respectively, the rate constants for the primary nucleation, fibril growth, and fragmentation. One of the experimental plots for each seed concentration that is the nearest to the logarithmic fitted curve in Fig. 4 (e) is also shown. Moreover, the relationship between the seed concentration and t_{half} with different (c) k_- and (d) k_n is presented. In the calculation, we used the rate constants of $k_n = 2.41 \times 10^{-14}$ $M^{-1} \cdot s^{-1}, k_+ = 9.92 \times 10^5 M^{-1} \cdot s^{-1},$ and $k_- = 9.68 \times 10^{-10} s^{-1}$. The t_{half} of the monomer solution is expediently plotted at a seed concentration of 10^{-20} M in Fig. 5 (c) and (d). The inset in (d) show the relationship between k_n and the seed detection limit (SDL), demonstrating that the increase in k_n deteriorates the SDL. (e) Schematic illustration of the mechanism of the accelerative amyloid fibril assay in the HANABI-2000; the red thunder motifs represent the enhanced pathways by ultrasonication.

value, regardless of ultrasonication. These results indicate that ultrasonication accelerates fibril formation by enhancing primary nucleation and fragmentation, but not fibril growth.

In the seed detection assay, enhancement of the fragmentation pathway effectively accelerates it, as shown in Fig. 5(c). The increase in k_- shortens the t_{half} for each seed concentration without affecting the SDL. In the calculation, the SDL is defined as a seed concentration in which the logarithmically-fitted curve of t_{half} reaches the t_{half} of the monomer solution, as explained by the broken lines in Fig. 5(c). In the case of $k_- = 9.68 \times 10^{-10}$ s^{-1}, SDL is approximately 2×10^{-18} M. Zeiger and Suslick reported that the dominant factor in fragmentation by ultrasonication is a shockwave generated by the bubble collapse in the fragmentation of aspirin crystals[44]. Furthermore, it has been reported that the hydrophobic residues at the fibril surface work as a nucleus of the cavitation bubble[45], which enhances the fibrils' fragmentation efficiency. Following the ultrasonic fragmentation, the fibrils' lengths depend on the number of ultrasonic pulses[46], demonstrating that fibril fragmentation is sensitive to the acoustic conditions.

In contrast, enhancement of the primary nucleation decreases the SDL, as shown in Fig. 5(d), which makes it unfavorable for further improvement of the SDL. As a microscopic mechanism, we previously found that transient cavitation is important for accelerating primary nucleation[23,47]. Without ultrasonication, primary nucleation stochastically occurs through the monomer collision due to the thermal fluctuation, which constitutes to homogeneous nucleation in the bulk solution. With ultrasonication, the cavitation bubbles produce the air–water interfaces in the solution. The denatured protein monomers, such as β_2m under acidic conditions, expose their hydrophobic amino acid residues to a solvent, which are attached on the air–water interface [48]. Thus, the cavitation bubbles function as the site of heterogeneous nucleation, which occurs with a lower free-energy barrier than that of the homogeneous one[49]. In addition to the aforementioned effect, the transient cavitation induces the further local condensation of the molecules and local temperature increase through the collapse event, drastically enhancing primary nucleation via the dual effect[23]. Although the primary nucleation enhancement is unfavorable in the seed detection assay, it is vital for investigating the nucleation propensity of samples without seeds.

The reaction scheme of the accelerative amyloid-fibril assays in the HANABI-2000 is summarized in Fig. 5(e). In terms of the seed detection, the ultra-trace seeds are rapidly amplified through the enhancement of the fragmentation. Additionally, ultrasonication promotes primary nucleation via the ultrasonic cavitation bubbles. The enhancement of the primary nucleation is undesirable in the seed detection, as it deteriorates the SDL by creating the seed-independent fibrils. Thus, it is important to explore the acoustic condition, which only accelerates the fragmentation but does not induce primary nucleation, in order to improve the SDL. However, from a different perspective, the primary nucleation enhancement is fairly valuable for investigating the risk of fibril formation, which is usually obscured by a high free-energy barrier of supersaturation. Our results demonstrate the applicability of the HANABI-2000, not only for accelerative seed detection but also for testing of the fibril-formation risk prior to the primary nucleation.

4. Conclusions

We developed the optimized sonoreactor, the HANABI-2000, for conducting the accelerative amyloid-fibril assays. To perform a reproducible assay, a water bath was eliminated from the sonoreactor. A single rod-shaped PZT transducer is placed in each sample solution, driven by separately setting the applied voltage and frequency through acoustic measurement. By compensating for the applied voltage, the HANABI-2000 induced β2m fibril formation in 36 samples with a CV in t_{half} of 21.8%, which is a reasonable value for uniform fibril formation. In the seed detection, the t_{half} of the solution with 100 fM seeds was clearly separated from a pure monomer solution. The time for seed detection was shortened by ultrasonication. Further analysis of the acceleration mechanism reveals that the accelerative amyloid-fibril assay is based on enhancing the primary nucleation and the fibril fragmentation. Our results substantiate the applicability of the HANABI-2000 in clinical situations for the accelerative seed detection and the further early-stage diagnosis of amyloidoses prior to the nucleation.

CRediT authorship contribution statement

Kichitaro Nakajima: Validation, Writing - original draft, Funding acquisition, Methodology, Formal analysis. **Kentaro Noi:** Methodology, Writing - review & editing. **Keiichi Yamaguchi:** Methodology, Validation, Formal analysis. **Masatomo So:** Methodology, Writing - review & editing. **Kensuke Ikenaka:** Validation, Investigation. **Hideki Mochizuki:** Validation, Funding acquisition, Writing - review & editing. **Hirotsugu Ogi:** Conceptualization, Methodology, Writing - review & editing, Funding acquisition. **Yuji Goto:** Conceptualization, Methodology, Writing - review & editing, Funding acquisition, Project administration.

Declaration of Competing Interest

The authors declare that they have no known competing financial interests or personal relationships that could have appeared to influence the work reported in this paper.

Acknowledgement

References

[1] D.S. Eisenberg, M.R. Sawaya, Structural studies of amyloid proteins at the molecular level, Annu. Rev. Biochem. 86 (2017) 69–95.

[2] F. Chiti, C.M. Dobson, Protein misfolding, functional amyloid, and human disease, Annu. Rev. Biochem. 75 (2006) 333–366.

[3] M. Bucciantini, E. Giannoni, F. Chiti, F. Baroni, N. Taddei, G. Ramponi, C. M. Dobson, M. Stefani, Inherent toxicity of aggregates implies a common mechanism for protein misfolding diseases, Nature 416 (2002) 507–511.

[4] A. Lorenzo, B.A. Yankner, Beta-amyloid neurotoxicity requires fibril formation and is inhibited by congo red, Proc. Natl. Acad. Sci. U.S.A. 91 (1994) 12243–12247.

[5] C. Liu, M. Zhao, L. Jiang, P.-N. Cheng, J. Park, M.R. Sawaya, A. Pensalfini, D. Gou, A.J. Berk, C.G. Glabe, J. Nowick, D. Eisenberg, Out-of-register β-sheets suggest a pathway to toxic amyloid aggregates, Proc. Natl. Acad. Sci. U.S.A. 109 (2012) 20913–20918.

[6] R.J. Bateman, C. Xiong, T.L. Benzinger, A.M. Fagan, A. Goate, N.C. Fox, D. S. Marcus, N.J. Cairns, X. Xie, T.M. Blazey, D.M. Holtzman, A. Santacruz, V. Buckles, A. Oliver, K. Moulder, P.S. Aisen, B. Ghetti, W.E. Klunk, E. McDade, R. N. Martins, C.L. Masters, R. Mayeux, J.M. Ringman, M.N. Rossor, P.R. Schofield, R. A. Sperling, S. Salloway, J.C. Morris, Clinical and biomarker changes in dominantly inherited Alzheimer's disease, N. Engl. J. Med. 367 (2012) 795–804.

[7] A.M. Morris, M.A. Watzky, J.N. Agar, R.G. Finke, Fitting neurological protein aggregation kinetic data via a 2-step, minimal/'Ockham's razor' model: The Finke-Watzky mechanism of nucleation followed by autocatalytic surface growth, Biochemistry 47 (2008) 2413–2427.

[8] J. Nývlt, Kinetics of nucleation in solutions, J. Cryst. Growth 3–4 (1968) 377–383.

[9] G. Coquerel, Crystallization of molecular systems from solution: phase diagrams, supersaturation and other basic concepts, Chem. Soc. Rev. 43 (2014) 2286–2300.

[10] J.T. Jarrett, P.T. Lansbury, Seeding 'one-dimensional crystallization' of amyloid: A pathogenic mechanism in Alzheimer's disease and scrapie? Cell 73 (6) (1993) 1055–1058.

[11] H. Naiki, K. Nakakuki, First-order kinetic model of Alzheimer's beta-amyloid fibril extension in vitro, Lab. Invest. 74 (1996) 374–383.

[12] T. Ban, K. Yamaguchi, Y. Goto, Direct observation of amyloid fibril growth, propagation, and adaptation, Acc. Chem. Res. 39 (2006) 663–670.

[13] T. Ikenoue, Y.-H. Lee, J. Kardos, H. Yagi, T. Ikegami, H. Naiki, Y. Goto, Heat of supersaturation-limited amyloid burst directly monitored by isothermal titration calorimetry, Proc. Natl. Acad. Sci. U.S.A. 111 (2014) 6654–6659.

[14] N. Salvadores, M. Shahnawaz, E. Scarpini, F. Tagliavini, C. Soto, Detection of misfolded Aβoligomers for sensitive biochemical diagnosis of Alzheimer's disease, Cell Rep. 7 (2014) 261–268.

[15] M.A. Metrick, N. do Carmo Ferreira, E. Saijo, A.G. Hughson, A. Kraus, C. Orrú, M. W. Miller, G. Zanusso, B. Ghetti, M. Vendruscolo, B. Caughey, Million-fold sensitivity enhancement in proteopathic seed amplification assays for biospecimens by Hofmeister ion comparisons, Proc. Natl. Acad. Sci. U.S.A. 116 (2019) 23029–23039.

[16] M. Shahnawaz, A. Mukherjee, S. Pritzkow, N. Mendez, P. Rabadia, X. Liu, B. Hu, A. Schmeichel, W. Singer, G. Wu, A.L. Tsai, H. Shirani, K.P.R. Nilsson, P.A. Low, C. Soto, Discriminating α-synuclein strains in Parkinson's disease and multiple system atrophy, Nature 578 (2020) 273–277.

[17] J. Bieschke, J. Russ, R.P. Friedrich, D.E. Ehrnhoefer, H. Wobst, K. Neugebauer, E. E. Wanker, EGCG remodels mature α-synuclein and amyloid-βfibrils and reduces cellular toxicity, Proc. Natl. Acad. Sci. U.S.A. 107 (17) (2010) 7710–7715.

[18] J. Habchi, S. Chia, C. Galvagnion, T.C. Michaels, M.M. Bellaiche, F.S. Ruggeri, M. Sanguanini, I. Idini, J.R. Kumita, E. Sparr, S. Linse, C.M. Dobson, T.P. Knowles, M. Vendruscolo, Cholesterol catalyses Aβ42 aggregation through a heterogeneous nucleation pathway in the presence of lipid membranes, Nat. Chem. 10 (6) (2018) 673–683.

[19] Y. Ohhashi, M. Kihara, H. Naiki, Y. Goto, Ultrasonication-induced amyloid fibril formation of β2-microglobulin, J. Biol. Chem. 280 (2005) 32843–32848.

[20] M. So, H. Yagi, K. Sakurai, H. Ogi, H. Naiki, Y. Goto, Ultrasonication-dependent acceleration of amyloid fibril formation, J. Mol. Biol. 412 (4) (2011) 568–577.

[21] A. Umemoto, H. Yagi, M. So, Y. Goto, High-throughput analysis of ultrasonication-forced amyloid fibrillation reveals the mechanism underlying the large fluctuation in the lag time, J. Biol. Chem. 289 (2014) 27290–27299.

[22] S. Nomura, K. Murakami, Y. Sasaki, Streaming induced by ultrasonic vibration in a water vessel, Jpn. J. Appl. Phys. 39 (2000) 3636–3640.

[23] K. Nakajima, H. Ogi, K. Adachi, K. Noi, M. Hirao, H. Yagi, Y. Goto, Nucleus factory on cavitation bubble for amyloid βfibril, Sci. Rep. 6 (2016) 1–10.

[24] K. Nakajima, M. So, K. Takahashi, Y.-I. Tagawa, M. Hirao, Y. Goto, H. Ogi, Optimized ultrasonic irradiation finds out ultrastable Aβ1-40 oligomers, J. Phys. Chem. B 121 (2017) 2603–2613.

[25] M. Hoshino, H. Katou, Y. Hagihara, K. Hasegawa, H. Naiki, Y. Goto, Mapping the core of the β2-microglobulin amyloid fibril by H/D exchange, Nat. Struct. Biol. 9 (2002) 332–336.

[26] T. Le Marchand, M. De Rosa, N. Salvi, B.M. Sala, L.B. Andreas, E. Barbet-Massin, P. Sormanni, A. Barbiroli, R. Porcari, C. Sousa Mota, D. De Sanctis, M. Bolognesi, L. Emsley, V. Bellotti, M. Blackledge, C. Camilloni, G. Pintacuda, S. Ricagno, Conformational dynamics in crystals reveal the molecular bases for D76N beta-2 microglobulin aggregation propensity, Nat. Commun. 9 (2018) 1–11.

[27] Y. Goto, H. Ogi, M. So, K. Ikenaka, H. Mochizuki, S. Hashimoto, Ultrasound generation member, ultrasound emission device, and ultrasonic modification observation devise, wo2019003601 (2019).

[28] H. Naiki, K. Higuchi, M. Hosokawa, T. Takeda, Fluorometric determination of amyloid fibrils in vitro using the fluorescent dye, thioflavine T, Anal. Biochem. 177 (1989) 244–249.

[29] T. Chiba, Y. Hagihara, T. Higurashi, K. Hasegawa, H. Naiki, Y. Goto, Amyloid fibril formation in the context of full-length protein: Effects of proline mutations on the amyloid fibril formation of β2-microglobulin, J. Biol. Chem. 278 (2003) 47016–47024.

[30] S.K. Maji, M.H. Perrin, M.R. Sawaya, S. Jessberger, K. Vadodaria, R.A. Rissman, P. S. Singru, K.P.R. Nilsson, R. Simon, D. Schubert, D. Eisenberg, J. Rivier, P. Sawchenko, W. Vale, R. Riek, Functional amyloids as natural storage of peptide hormones in pituitary secretory granules, Science 325 (2009) 328–332.

[31] H. Yagi, K. Hasegawa, Y. Yoshimura, Y. Goto, Acceleration of the depolymerization of amyloid βfibrils by ultrasonication, Biochim. Biophys. Acta 2013 (1834) 2480–2485.

[32] T.P.J. Knowles, C.A. Waudby, G.L. Devlin, S.I.A. Cohen, A. Aguzzi, M. Vendruscolo, E.M. Terentjev, M.E. Welland, C.M. Dobson, An analytical solution to the kinetics of breakable filament assembly, Science 326 (2009) 1533–1537.

[33] K. Uesugi, H. Ogi, M. Fukushima, M. So, H. Yagi, Y. Goto, M. Hirao, Mechanisms of ultrasonically induced fibrillation of amyloid β1−40 peptides, Jpn. J. Appl. Phys. 52 (2013) 07HE10.

[34] Y. Yoshimura, Y. Lin, H. Yagi, Y.-H. Lee, H. Kitayama, K. Sakurai, M. So, H. Ogi, H. Naiki, Y. Goto, Distinguishing crystal-like amyloid fibrils and glass-like amorphous aggregates from their kinetics of formation, Proc. Natl. Acad. Sci. U.S. A. 109 (2012) 14446–14451.

[35] M. Adachi, M. So, K. Sakurai, J. Kardos, Y. Goto, Supersaturation-limited and unlimited phase transitions compete to produce the pathway complexity in amyloid fibrillation, J. Biol. Chem. 290 (2015) 18134–18145.

[36] S. Noda, M. So, M. Adachi, J. Kardos, Y. Akazawa-Ogawa, Y. Hagihara, Y. Goto, Thioflavin T-silent denaturation intermediates support the main-chain-dominated architecture of amyloid fibrils, Biochemistry 55 (2016) 3937–3948.

[37] J. Hoshino, K. Yamagata, S. Nishi, S. Nakai, I. Masakane, K. Iseki, Y. Tsubakihara, Significance of the decreased risk of dialysis-related amyloidosis now proven by results from Japanese nationwide surveys in 1998 and 2010, Nephrol. Dial. Transpl. 31 (2015) 595–602.

[38] A.K. Buell, C. Galvagnion, R. Gaspar, E. Sparr, M. Vendruscolo, T.P.J. Knowles, S. Linse, C.M. Dobson, Solution conditions determine the relative importance of nucleation and growth processes in α-synuclein aggregation, Proc. Natl. Acad. Sci. U.S.A. 111 (2014) 7671–7676.

[39] M. Shahnawaz, T. Tokuda, M. Waragai, N. Mendez, R. Ishii, C. Trenkwalder, B. Mollenhauer, C. Soto, Development of a Biochemical Diagnosis of Parkinson Disease by Detection of α-Synuclein Misfolded Aggregates in Cerebrospinal Fluid, JAMA Neurology 74 (2017) 163–172.

[40] E.K. Hill, B. Krebs, D.G. Goodall, G.J. Howlett, D.E. Dunstan, Shear flow induces amyloid fibril formation, Biomacromolecules 7 (2006) 10–13.

[41] M. Törnquist, T.C.T. Michaels, K. Sanagavarapu, X. Yang, G. Meisl, S.I.A. Cohen, T. P.J. Knowles, S. Linse, Secondary nucleation in amyloid formation, Chem. Commun. 54 (2018) 8667–8684.

[42] J. Hofrichter, P.D. Ross, W.A. Eaton, Supersaturation in sickle cell hemoglobin solutions, Proc. Natl. Acad. Sci. U.S.A. 73 (1976) 3035–3039.

[43] M. So, D. Hall, Y. Goto, Revisiting supersaturation as a factor determining amyloid fibrillation, Curr. Opin. Struct. Biol. 36 (2016) 32–39.

[44] B.W. Zeiger, K.S. Suslick, Sonofragmentation of molecular crystals, J. Am. Chem. Soc. 133 (2011) 14530–14533.

[45] H. Okumura, S.G. Itoh, Amyloid fibril disruption by ultrasonic cavitation: Nonequilibrium molecular dynamics simulations, J. Am. Chem. Soc. 136 (2014) 10549–10552.

[46] E. Chatani, Y.-H. Lee, H. Yagi, Y. Yoshimura, H. Naiki, Y. Goto, Ultrasonication-dependent production and breakdown lead to minimum-sized amyloid fibrils, Proc. Natl. Acad. Sci. U.S.A. 106 (2009) 11119–11124.

[47] K. Nakajima, D. Nishioka, M. Hirao, M. So, Y. Goto, H. Ogi, Drastic acceleration of fibrillation of insulin by transient cavitation bubble, Ultrason. Sonochem. 36 (2017) 206–211.

[48] L. Jean, C. Lee, D. Vaux, Enrichment of amyloidogenesis at an air-water interface, Biophys. J. 102 (5) (2012) 1154–1162.

[49] A.K. Srivastava, J.M. Pittman, J. Zerweck, B.S. Venkata, P.C. Moore, J. R. Sachleben, S.C. Meredith, β-Amyloid aggregation and heterogeneous nucleation, Protein Sci. 28 (2019) 1567–1581.